Journal of Colloid and Interface Science 325 (2008) 516–525

Contents lists available at ScienceDirect

Journal of Colloid and Interface Science

www.elsevier.com/locate/jcis

Electrophoresis of a charge-regulated sphere at an arbitrary position in a charged spherical cavity

J.P. Hsu [a,*], C.Y. Chen [a], Duu-Jong Lee [a], Shiojenn Tseng [b], Ay Su [c]

[a] Department of Chemical Engineering, National Taiwan University, Taipei 10617, Taiwan
[b] Department of Mathematics, Tamkang University, Tamsui, Taipei 25137, Taiwan
[c] Department of Mechanical Engineering & Fuel Cells Research Center, Yuan Ze University, 135 Yuan-Tung Road, Chung Li, Tao Yuan 320, Taiwan

ARTICLE INFO

Article history:
Received 16 April 2008
Accepted 20 May 2008
Available online 1 July 2008

Keywords:
Electrophoresis
Boundary effect
Charge-regulated sphere
Charged spherical cavity
Electroosmotic flow

ABSTRACT

The electrophoresis of a charge-regulated spherical particle at an arbitrary position in a charged spherical cavity is modeled under conditions of low surface potential (<25 mV) and weak applied electric field (<25 kV/m). The charged cavity allows us to simulate the effect of electroosmotic flow, and the charge-regulated nature of the particle permits us to model various types of surface. The problem studied previously is reanalyzed based on a more rigorous electric force formula. In particular, the influences of various types of charged conditions on the electrophoretic behavior of a particle and the roles of all the relevant forces acting on the particle are examined in detail. Several new results are found. For instance, the mobility of a particle has a local minimum as the thickness of a double layer varies, which is not seen in the cases where the surface of a particle is maintained at a constant potential and at a constant charge density.

1. Introduction

Boundary effect is one of the key factors that are of practical significance in electrophoresis operation. This effect can influence the electrophoretic behavior of a particle both qualitatively and quantitatively [1–3]. Among various types of boundary assumed in theoretical analyses, the spherical cavity proposed by Zydney [4] is simple in structure but is capable of modeling the boundary effect appropriately under certain conditions [5–7]. The geometry of a sphere in a spherical cavity has been adopted by many researchers for studies of boundary effects on the electrophoretic behavior of a particle [4–10].

In a study of the electrophoresis of a charge-regulated particle in a spherical cavity, Yu et al. [6] found that if both the surface of a particle and that of a cavity are kept at constant potential, then the mobility of the particle may have a local minimum as its position in the cavity varies. A similar result was also observed in Hsu et al. [9]. This behavior was explained by charge reversal as a particle is sufficiently close to a cavity. In these studies, the evaluation of the electric force acting on a particle was based on the total potential, which includes the equilibrium potential and the potential that arises from the applied electric field. Although this approach has been adopted by many investigators, we showed recently that for a non-totally-symmetric geometry, it is more realistic to exclude the driving force contributed by the equilibrium potential [11,12]. In an attempt to provide more a rigorous explanation for the electrophoretic behavior of a particle near a boundary, the problem considered by Yu et al. [6] is reanalyzed in this study. In particular, the influence of various types of charged conditions on the electrophoretic behavior of a particle and the roles of all the relevant forces acting on a particle are examined in detail.

2. Materials and methods

Let us consider the problem illustrated in Fig. 1, where a nonconductive spherical particle of radius a is at an arbitrary position in a nonconductive spherical cavity of radius b. The surface of the particle bears an acidic function group AH, which is capable of undergoing the dissociation reaction expressed by

$$AH \Leftrightarrow A^- + H^+. \tag{1}$$

The equilibrium constant of this reaction, K_a, is expressed by

$$K_a = \frac{[A^-]_s (H^+)_s}{[AH]_s}, \tag{2}$$

where $[A^-]_s$ and $[AH]_s$ are the number densities of A^- and AH on the particle surface, respectively, and $(H^+)_s$ is the surface concentration of H^+. The cavity is filled with an incompressible Newtonian fluid of constant physical properties containing electrolytes.

* Corresponding author. Fax: +886 2 23623040.
E-mail address: jphsu@ntu.edu.tw (J.P. Hsu).

0021-9797/$ – see front matter
doi:10.1016/j.jcis.2008.05.036

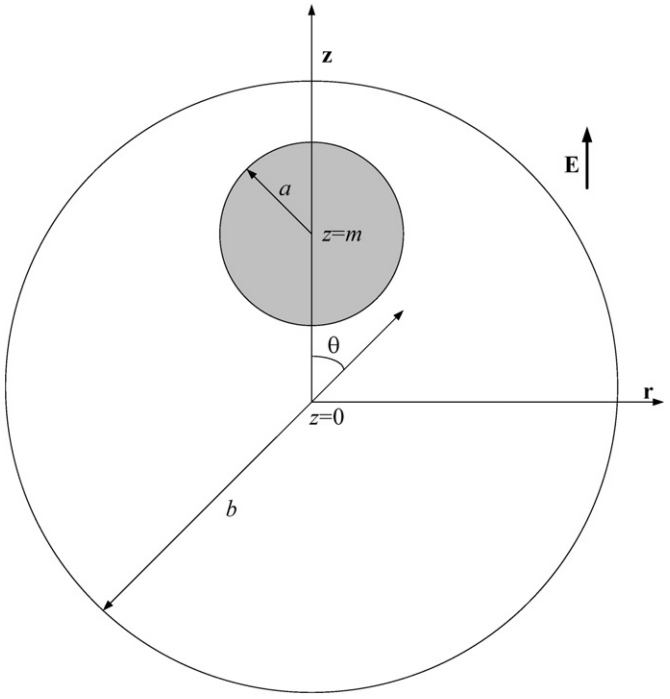

Fig. 1. The electrophoresis of a charged, nonconductive spherical particle of radius $a$at an arbitrary position in a spherical cavity of radius b, where (r, θ, z) are the cylindrical coordinates with the origin at the center of the cavity, **E** is an applied uniform electric field in the z-direction, and the center of the sphere is at $z = m$.

The cylindrical coordinates (r, θ, z) are adopted with the origin located at the center of the cavity. The center of the particle is at $z = m$. A uniform electric field **E** pointed in the z-direction with strength E is applied. Because the system is symmetric about θ, only the (r, z) domain needs to be considered. Assuming steady state, the governing equations of the present problem can be summarized as follows [13]:

$$\nabla^2\Psi = -\frac{\rho_e}{\varepsilon} = -\sum_j \frac{z_j e n_j}{\varepsilon}, \tag{3}$$

$$\nabla \cdot \mathbf{u} = 0, \tag{4}$$

$$\eta\nabla^2\mathbf{u} - \nabla p = -\rho_e \mathbf{E}. \tag{5}$$

Here, Ψ, ∇^2, ε, ρ_e, n_j, z_j, and e are the electrical potential, the Laplacian, the dielectric constant of the liquid phase, the space charge density, the bulk number concentration and the valence of ionic species j, and the elementary charge, respectively. **u**, η, and p are the fluid velocity, the viscosity, and the pressure, respectively.

Suppose that **E** is a weak electric field relative to that established by the particle and/or the cavity, and the surface potential of the particle and/or that of the cavity is low. The former is reasonable if E is lower than ca. 25 kV/m, and the latter is satisfied if the surface potential is lower than ca. 25 mV [11]. Under these conditions, Eq. (3) can be replaced by [14]

$$\nabla^2\Psi_1 = \kappa^2\Psi_1, \tag{6}$$

$$\nabla^2\Psi_2 = 0, \tag{7}$$

where $\Psi = \Psi_1 + \Psi_2$, Ψ_1 is the electrical potential in the absence of E or the equilibrium potential, and Ψ_2 is the electrical potential outside the particle arising from **E**, $\mathbf{E} = -\nabla\Psi_2$.

$$\kappa = \Big[\sum_j n_j^0 (e z_j)^2/\varepsilon k_B T\Big]^{1/2}$$

is the reciprocal Debye length, n_j^0, k_B, and T being the bulk number concentration of ionic species j, the Boltzmann constant, and the absolute temperature. The boundary conditions associated with Eqs. (6) and (7) are assumed to be

$$\mathbf{n}\cdot\nabla\Psi_1 = -\frac{\sigma_p}{\varepsilon} \quad \text{and} \quad \mathbf{n}\cdot\nabla\Psi_2 = 0 \quad \text{on the particle surface,} \tag{8}$$

$$\Psi_1 = \zeta_w \quad \text{and} \quad \mathbf{n}\cdot\nabla\Psi_2 = -E_z\cos\theta \quad \text{on the cavity surface,} \tag{9}$$

where σ_p is the surface charge density of the particle, ζ_w is the surface potential of the cavity, **n** is the unit normal vector pointing to the liquid phase, and E_z is the z-component of **E**.

Assuming Boltzmann distribution for the spatial variation of the molar concentration of H^+, it can be shown that [3]

$$\sigma_p = -\frac{eN_s}{1 + \frac{C^0_{H^+}}{K_a}\exp(-\frac{e\zeta_p}{k_B T})}, \tag{10}$$

where N_s is the density of the acidic functional groups on the particle surface, ζ_p is the surface potential of the particle, and $C^0_{H^+}$ is the bulk concentration of H^+. If ζ_p is low, this expression can be approximated by

$$\sigma_p \cong \frac{-eN_s}{\{1 + C^0_{H^+}/K_a\}} - \frac{(e^2 N_s/k_B T)\{C^0_{H^+}/K_a\}}{\{1 + C^0_{H^+}/K_a\}^2}\zeta_p. \tag{11}$$

Suppose that both the surface of the particle and that of the cavity are no-slip. Then the boundary conditions associated with Eqs. (4) and (5) are

$$\mathbf{u} = U\mathbf{e}_z \quad \text{on the particle surface,} \tag{12}$$

$$u = 0 \quad \text{on the cavity surface.} \tag{13}$$

Here, U is the z-component of the particle velocity and $\mathbf{e}_z$ is the unit vector in the z-direction.

For the present case, the forces acting on the particle include the electric force $\mathbf{F}_E$ and the hydrodynamic force $\mathbf{F}_D$. If we let F_E and F_D be the z-components of these forces, then $F_E + F_D = 0$ at steady state. F_E and F_D can be evaluated by [1–3,14–17]

$$F_E = \iint_S \sigma_p E_z\, dS, \tag{14}$$

$$F_D = \iint_S \eta\frac{\partial(\mathbf{u}\cdot\mathbf{t})}{\partial n}t_z\, dS + \iint_S -pn_z\, dS, \tag{15}$$

where S is the surface of the particle, **t** the unit tangent vector on S, n the magnitude of **n**, and t_z and n_z are the z-components of **t** and **n**, respectively. For a simpler treatment, the problem under consideration is decomposed into two subproblems [18]. In the first subproblem the particle translates with a constant velocity U in the absence of **E**, and in the second subproblem **E** is applied but the particle is held fixed. In the first subproblem the particle experiences a conventional drag force $F_{D,1} = -UD$, where D is the drag coefficient. In the second subproblem the particle experiences both an electric force F_E and a hydrodynamic force $F_{D,2}$, which arises from the movement of the ionic species in the double layer surrounding the particle. The force balance $F_E + F_D = 0$ yields

$$U = \frac{F_E + F_{D,2}}{D}. \tag{16}$$

For convenience, the following scaled symbols are defined: P $(= 100m/(b-a)\%)$ is the scaled position of the particle; κa is the scaled thickness of the double layer; λ $(= a/b)$ is the scaled size of the cavity; $A = e^2 N_s a/\varepsilon k_B T$ is a parameter measuring the density of the acidic functional groups on the particle surface; $B = C^0_{H^+}/K_a$ is a parameter measuring the bulk concentration of H^+ (or pH); $U^* = U/U_{ref}$ is the scaled electrophoretic mobility,

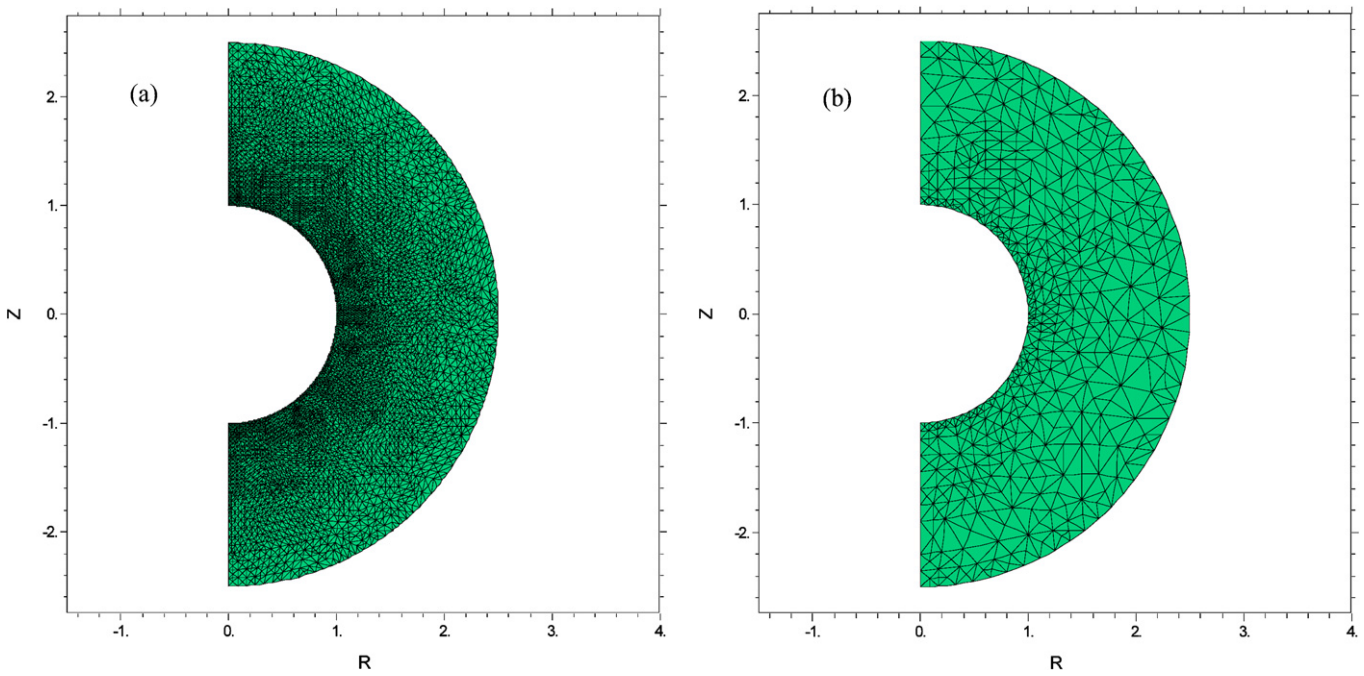

Fig. 2. Typical meshes used in the resolution of the electric field (a) and of the flow field (b) for an incompressible Newtonian fluid. Other parameters used are $\zeta_p^* = 1$, $\zeta_w^* = 0$, $A = 1$, $B = 1$, $\kappa a = 1$, $\lambda = 0.4$, and $P = 0\%$.

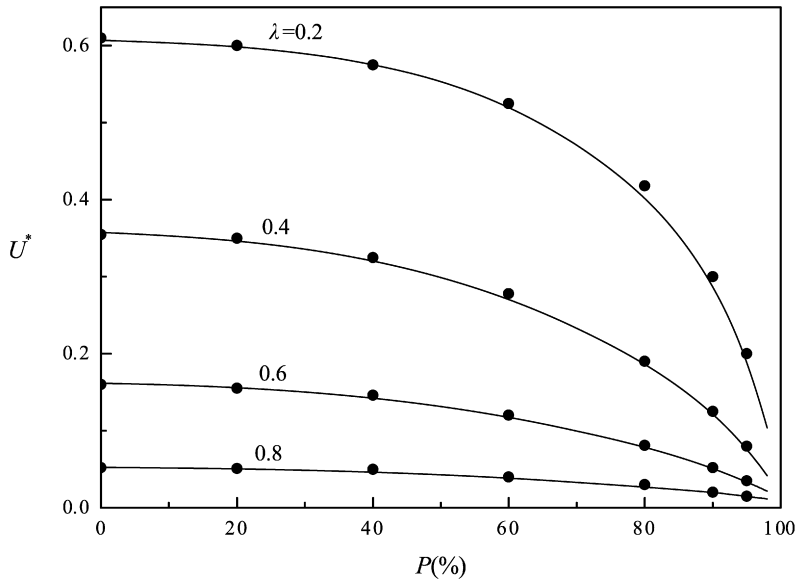

Fig. 3. Variation of the scaled mobility U^* as a function of P for various values of λ for the case of a positively charged sphere in an uncharged spherical cavity at $\zeta_p^* = 1$ and $\zeta_w^* = 0$. Solid curves, present results; discrete symbols, those of Hsu et al. [5].

where $U_{ref} = \varepsilon(k_B T/e)E_\infty/\eta$ is a reference velocity; $\zeta_w^* = e\zeta_w/k_B T$ is the scaled surface potential of the cavity; $F_E^* = F_E/6\pi\eta a U_{ref}$ and $F_{D,2}^* = F_{D,2}/6\pi\eta a U_{ref}$ are scaled forces; and $D^* = D/6\pi\eta a$ is the scaled drag coefficient.

3. Results and discussion

The governing equations and the associated boundary conditions are solved numerically by FlexPDE [19], which is based on a finite element scheme. In the numerical simulation, grid independence is checked to ensure that the mesh used is appropriate. In Fig. 2, the numbers of nodes necessary for the resolution of the electric field and the flow field are ca. 130,800 and 3669, respectively. To illustrate the performance of the software adopted, it is used to solve the problem considered by Hsu et al. [5], namely, the electrophoresis of a rigid sphere of constant surface potential in an uncharged spherical cavity. Fig. 3 presents the variation of the scaled mobility U^* as a function of P^* at various values of λ. As seen, the performance of the software adopted is satisfactory.

Note that Eqs. (11) and (8) lead to

$$\frac{1+B}{A}\frac{d\Psi_1^*}{dn} - \frac{B}{1+B}\Psi_1^* \cong 1 \quad \text{on the particle surface,} \tag{17}$$

where $\Psi_1^* = e\Psi_1/k_B T$ and n is the magnitude of $\mathbf{n}$. This expression implies that the two widely assumed conditions for the description of the surface of a charged particle, namely, constant potential and constant charge density, can be recovered from the present charge-regulation model by letting $A \to \infty$ and $B \to 0$, respectively.

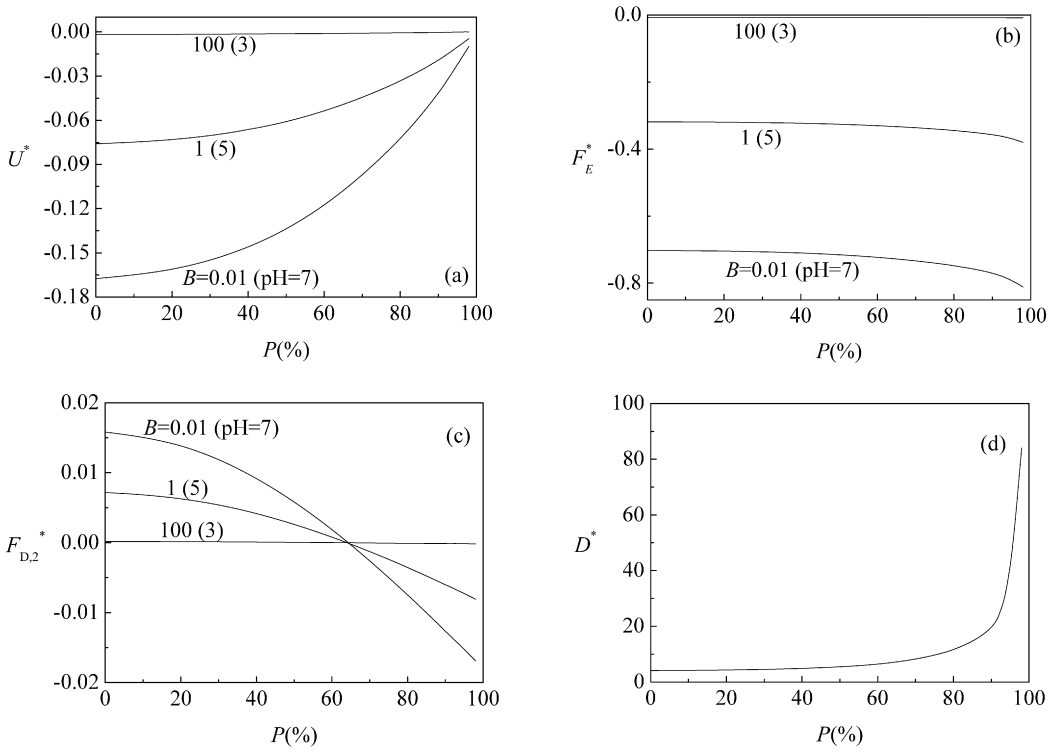

Fig. 4. Variation of the scaled mobility U^* (a), the electric force F_E^* (b), the scaled excess hydrodynamic force $F_{D,2}^*$ (c), and the scaled hydrodynamic force coefficient D^* (d) as functions of P for various values of B (or pH) at $A = 1$, $\zeta_w^* = 0$, $\kappa a = 1$, and $\lambda = 0.4$.

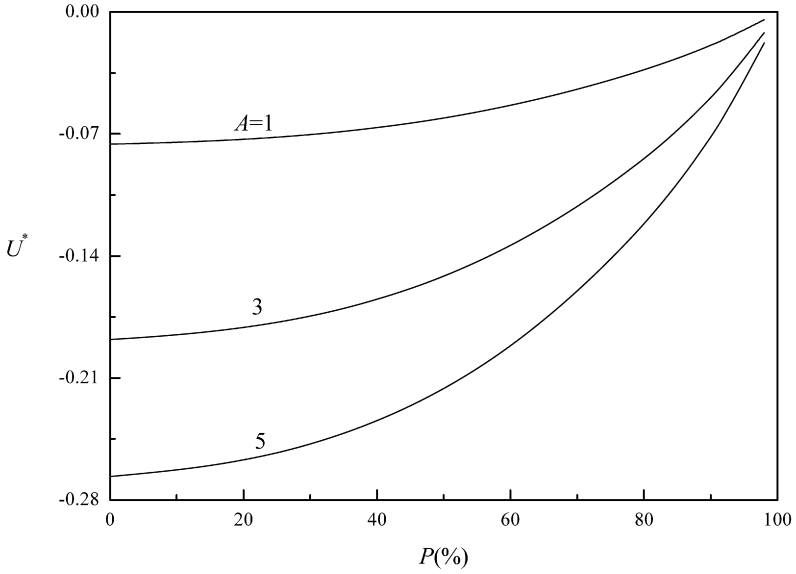

Fig. 5. Variation of the scaled mobility U^* as a function of P for various values of A at $B = 1$, $\zeta_w^* = 0$, $\kappa a = 1$, and $\lambda = 0.4$.

In subsequent discussions we consider three representative cases: a charge-regulated sphere in an uncharged cavity, a positively charged cavity, and a negatively charged cavity. For illustration, the radius of the particle a is fixed.

3.1. Charge-regulated sphere in an uncharged cavity

Let us consider first the case where a charge-regulated sphere is placed in an uncharged cavity. Fig. 4 illustrates the variations of the scaled mobility, U^*, and the corresponding scaled forces, F_E^*, $F_{D,2}^*$, and D^*, as functions of the position parameter P $(= 100m/(b-a)\%)$ at various levels of parameter B $(= C_{H^+}^0/K_a)$, or pH. U^* is seen to decline with increasing B because the greater the B the higher the bulk concentration of H^+, leading to a lower surface concentration of A^- and a smaller electrical driving force $|F_E^*|$, as illustrated in Fig. 4b [20]. Note that except for P close to 100%, F_E^* is the dominating force in this case. If P exceeds ca. 90%, $D^* \gg (|F_E^* + F_{D,2}^*|)$, implying that the retardation arising from the presence of the cavity dominates. In this case, $|U^*|$ declines rapidly with increasing P, and vanishes at $P = 100\%$, as required by the nonslip boundary condition assumed for the flow field.

Fig. 5 indicates that the absolute value of the scaled mobility, $|U^*|$, increases with increased A $(= e^2 N_s a/\varepsilon kT)$. This is because the greater the A the larger the number of acidic functional groups

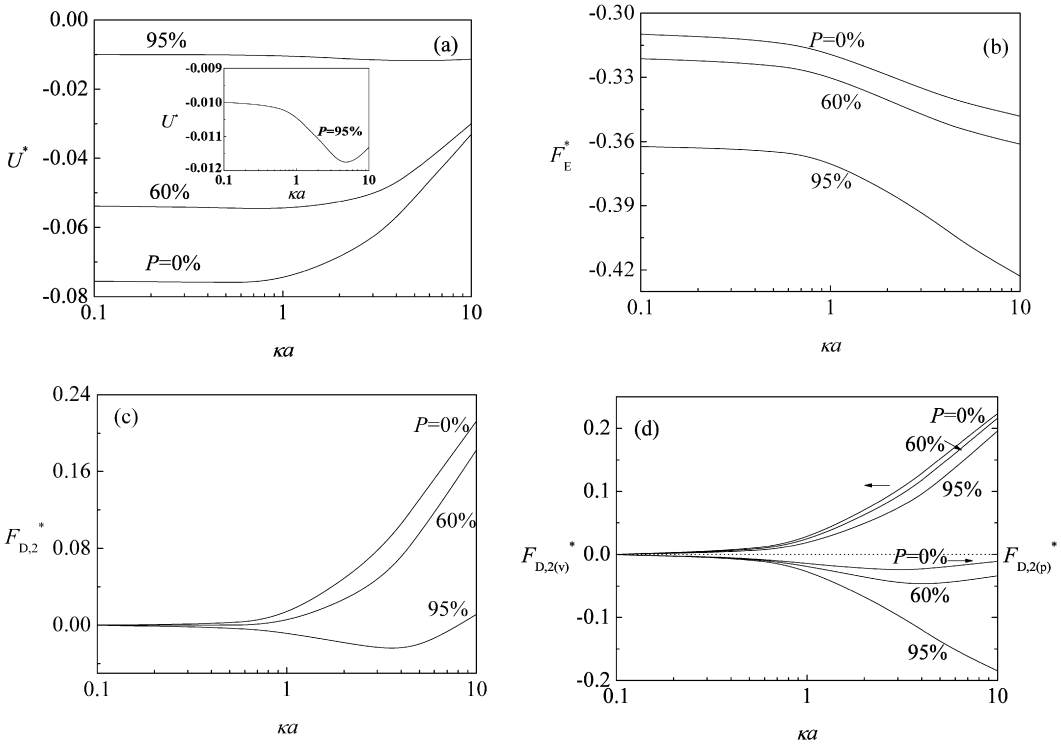

Fig. 6. Variation of scaled mobility U^* (a), the electric force F_E^* (b), scaled excess hydrodynamic force $F_{D,2}^*$ (c), and scaled excess hydrodynamic force $F_{D,2(v)}^*$ and $F_{D,2(P)}^*$ (d) as functions of κa for various P at $A = 1$, $B = 1$, $\zeta_w^* = 0$, and $\lambda = 0.4$.

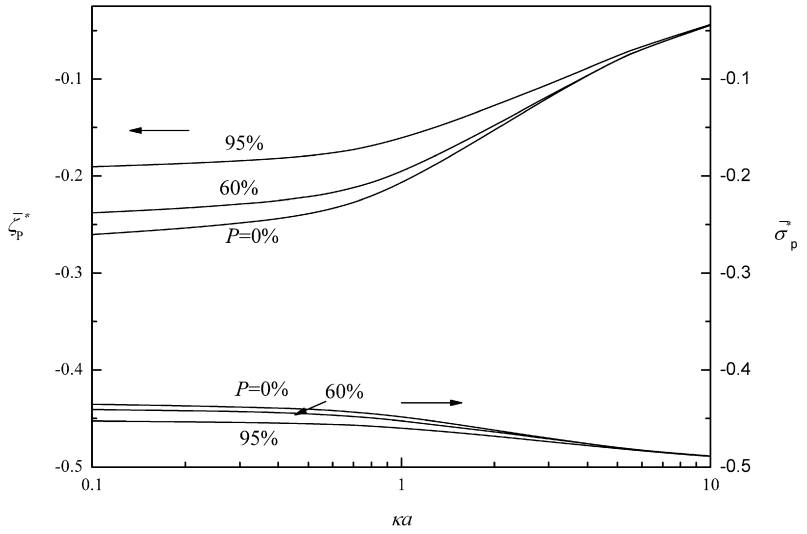

Fig. 7. Variations of the average scaled surface potential of the particle $\bar{\zeta}_p^*$ and the average surface charge density $\overline{\sigma_p}^*$ as functions of κa for various values of P at $A = 1$, $B = 1$, $\zeta_w^* = 0$, and $\lambda = 0.4$.

on the particle surface, leading to a higher surface charge density [3], and a greater scaled electrical driving force $|F_E^*|$. Again, F_E^* dominates except when P is close to 100%. As in Fig. 4, the rapid decrease in $|U^*|$ as P approaches 100% arises from the rapid increase in D^*.

The influence of the thickness of the double layer, measured by κa, on the scaled mobility, U^*, and the corresponding scaled forces, F_E^* and $F_{D,2}^*$, is illustrated in Fig. 6. Note that D^* is independent of κa. Fig. 6a reveals that if P is not large (0% and 60%), $|U^*|$ decreases monotonically with increasing κa, which is different from the behavior of a rigid sphere remaining at constant surface potential. Fig. 7 shows the variations of the average surface potential $\bar{\zeta}_p^*$ and the average surface charge density $\overline{\sigma_p}^*$ as a function of κa at various levels of P. Note that while $|\overline{\sigma_p}^*|$ increases with increasing κa, which is consistent with Fig. 6b, $|\bar{\zeta}_p^*|$ declines at the same time.

It is interesting to note that if P is sufficiently large (95%) U^* has a negative local minimum at $\kappa a \cong 5$. These results can be explained by the trends of F_E^* and $F_{D,2}^*$. According to Fig. 6b, $|F_E^*|$ increases with increasing κa, because the thinner the double layer the higher the surface charge density, as is pointed out for the electrophoresis of a rigid particle [5]. However, $F_{D,2}^*$, which is positive except when P is large, also increases with κa, as seen in Fig. 6c [3]. Note that $F_{D,2}^*$ comprises a viscous term, $F_{D,2(v)}^*$, and a pressure term, $F_{D,2(P)}^*$. The specific behavior of $F_{D,2}^*$ at $P = 95\%$, where it has a negative local minimum as κa varies, arises from

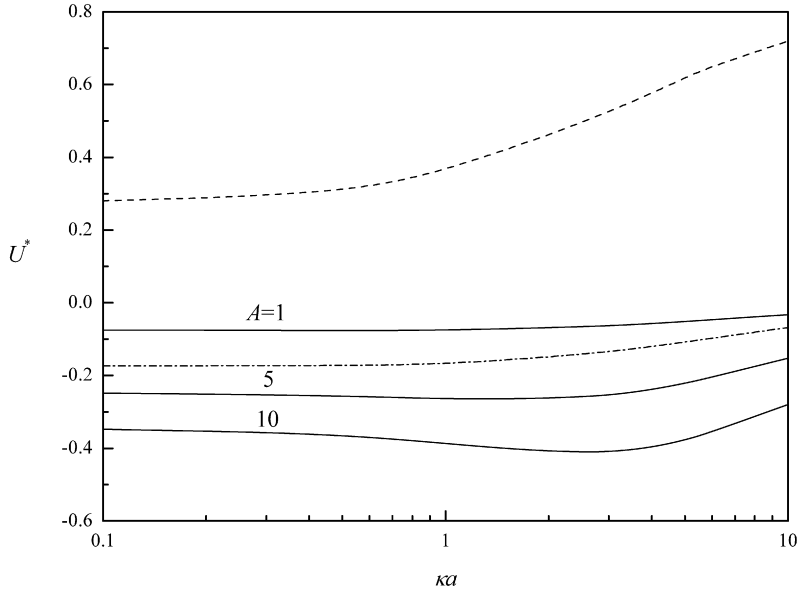

Fig. 8. Variations of the scaled mobility U^* as a function of κa for various types of charged conditions on the particle surface at $\zeta_w^* = 0$, $P = 0\%$, and $\lambda = 0.4$. Solid curves, charge-regulated surface at $B = 1$; (- - -) constant surface potential at $\zeta_p^* = 1$ [5]; (-·-·-·-) constant surface charge at $\sigma_p = 2.75 \times 10^{-15}$ C/m^2.

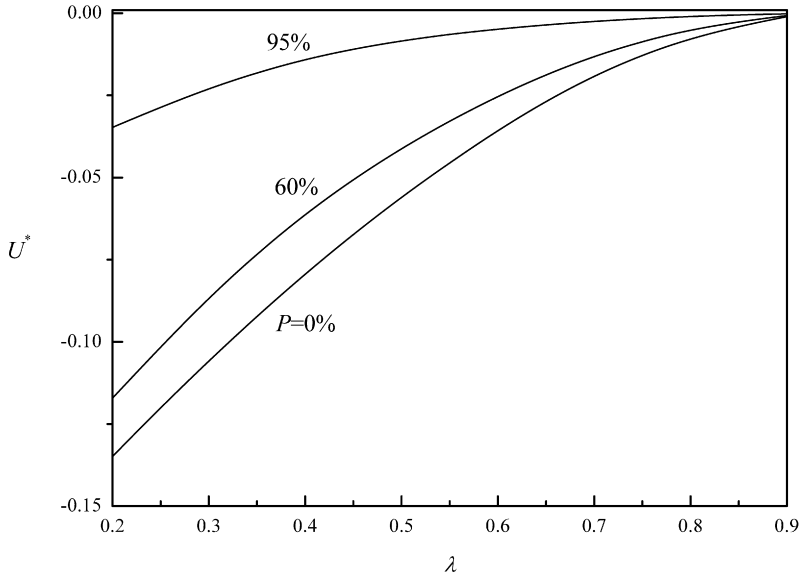

Fig. 9. Variation of the scaled mobility U^* as a function of λ for various values of P at $A = 1$, $B = 1$, $\zeta_w^* = 0$, and $\kappa a = 1$.

the competition of these two terms, shown in Fig. 6d. If κa is small and P is large (i.e., thick double layer and boundary effect important), then $F^*_{D,2(P)}$ dominates. On the other hand, if κa is large and P is small, $F^*_{D,2(v)}$ dominates [5,15,16].

A comparison between the electrophoretic behavior under various types of charged conditions is illustrated in Fig. 8. This figure reveals that if the surface of a particle is kept at constant potential, U^* increases monotonically with decreasing thickness of the double layer (increasing κa) [5]. On the other hand, if the surface of a particle is kept at constant charge density, $|U^*|$ decreases monotonically with decreasing thickness of the double layer. It is interesting to note that if the surface of a particle is of a charge-regulated nature, $|U^*|$ has a local maximum as κa varies.

Fig. 9 shows the influence of the scaled size of the cavity λ $(= a/b)$ on the scaled mobility of the particle, U^*. This figure indicates that $U^* \to 0$ as $P \to 100\%$ and/or $\lambda \to 1$. This is expected because the retardation due to the presence of the cavity, which is of a nonslip nature, becomes significant as P and/or λ increase.

3.2. Charge-regulated sphere in a positively charged cavity

Consider next the case where a charge-regulated sphere is in a positively charged cavity. In this case, the presence of the charged cavity yields a clockwise (counterclockwise) electroosmotic flow on the right-(left-)hand side of the particle. Because if the cavity is uncharged, the flow of the fluid near the particle is counterclockwise (clockwise) on its right-(left-)hand side, the presence of the electroosmotic flow has the effect of reducing the particle velocity. A comparison between Figs. 4c and 10b reveals that the $|F^*_{D,2}|$ for the present case is greater than that for the case where the cavity is uncharged, leading to a greater hydrodynamic force acting on the particle [4]. The competition between the hydrodynamic force and the electric force acting on the particle makes its

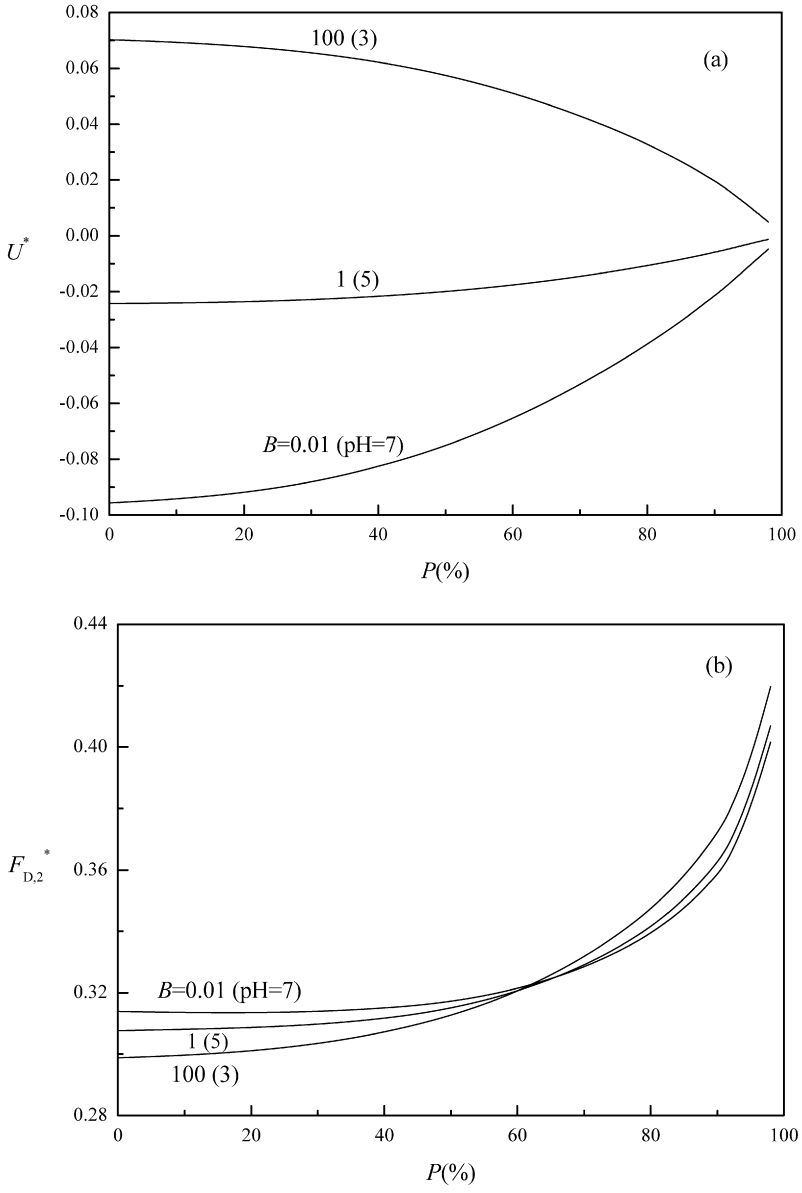

Fig. 10. Variation of the scaled mobility U^* (a), and the scaled electric force $F^*_{D,2}$ (b), as functions of P for various values of B (or pH) at $A = 1$, $\zeta^*_w = 1$, $\kappa a = 1$, and $\lambda = 0.4$.

electrophoretic behavior more complicated than that for the case where the cavity is uncharged. The variations of U^* and $F^*_{D,2}$ as a function of P at various levels of B are presented in Fig. 10. Note that in the present case F^*_E and D^* are the same as those shown in Figs. 4b and 4d, respectively. Fig. 10a reveals that if B is not large, U^* is negative and $|U^*|$ declines monotonically with increasing P. On the other hand, if B is sufficiently large, U^* is positive and U^* decreases monotonically with increasing P. The difference between the behavior of U^* shown in Fig. 10a and that in Fig. 4a arises mainly from the difference of the behavior of $F^*_{D,2}$ in these two case. In Fig. 10b, $F^*_{D,2}$ is always positive, and it increases with decreasing B and/or increasing P.

The behavior of U^* as A and/or P vary is similar to that observed in Fig. 5, that is, $|U^*|$ increases with increasing A and declines with increasing P, and can be explained by the same reasoning. Note that although negative charge is induced on the particle surface as it approaches the positively charged cavity, leading to a higher surface charge density and electrical driving force, the electroosmotic flow arising from the presence of the charged cavity has the effect of reducing the mobility of the particle. Therefore, the behavior of A is roughly the same as that shown in Fig. 5.

Fig. 11 reveals that if κa is small, U^* is negative and $|U^*|$ declines with increasing κa. On the other hand, if κa exceeds ca. unity, U^* becomes positive and U^* increases with increasing κa. This behavior can be explained by the behavior of F^*_E and $F^*_{D,2}$ as κa varies, presented in Figs. 11b and 11c. As seen in Fig. 9b, the smaller the κa the larger the $|F^*_E|$ because the smaller the κa the more important the electrical interaction between the particle and the cavity, and therefore, the greater the amount of negative charge induced on the particle surface. If κa exceeds ca. 4.5, the influence of the cavity on the particle is unimportant and the situation becomes similar to that for the case when the cavity is uncharged (Fig. 6b), where $|F^*_E|$ increases with increasing κa. The trend of $F^*_{D,2}$ seen in Fig. 11c arises from the competition between $F^*_{D,2(P)}$ and $F^*_{D,2(v)}$. If the boundary effect is important (small κa and/or large P), $F^*_{D,2}$ is dominated by $F^*_{D,2(P)}$; on the other hand, it is dominated by $F^*_{D,2(v)}$.

The variations of the scaled mobility, U^*, and the corresponding scaled forces, F^*_E, $F^*_{D,2}$, and D^*, as a function of the scaled size

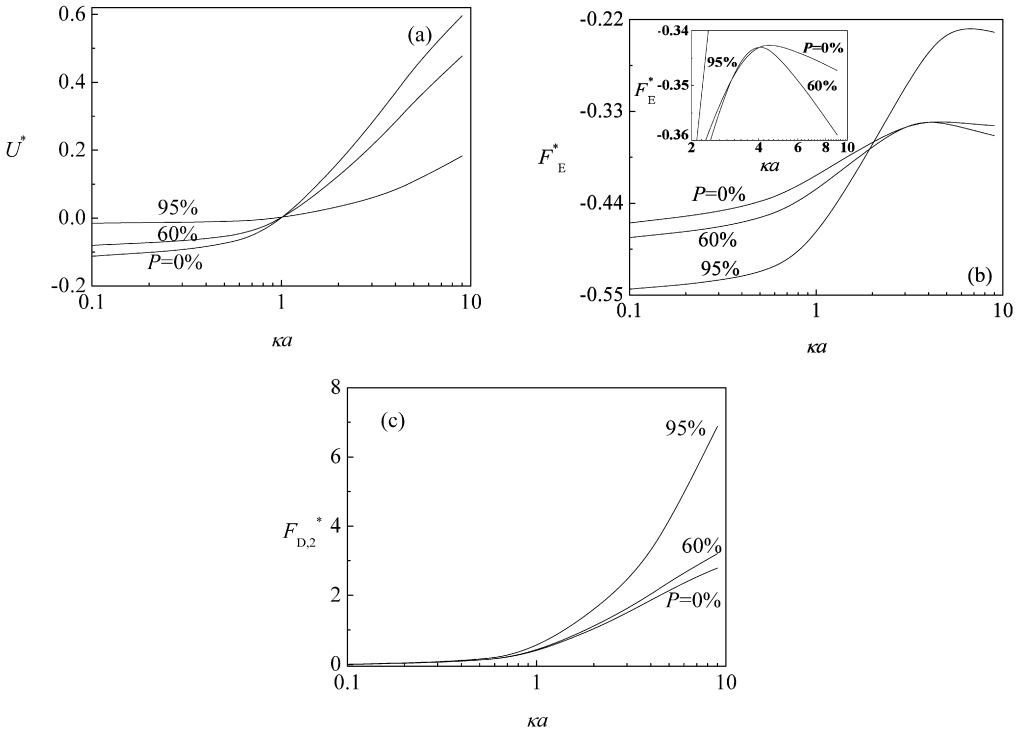

Fig. 11. Variation of the scaled mobility U^* (a), the scaled electric force F_E^* (b), and the scaled excess hydrodynamic force $F_{D,2}^*$ (c) as functions of κa for various values of P at $A = 1$, $B = 1$, $\zeta_w^* = 1$, and $\lambda = 0.4$.

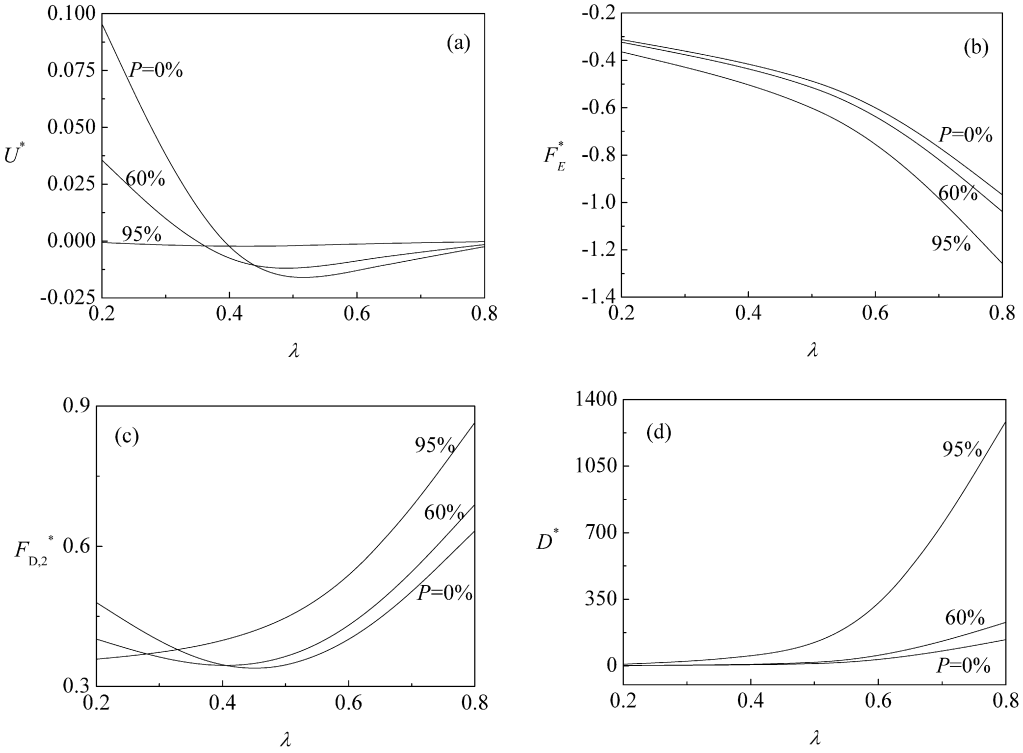

Fig. 12. Variation of the scaled mobility U^* (a), the scaled electric force F_E^* (b), the scaled excess hydrodynamic force $F_{D,2}^*$ (c), and the scaled hydrodynamic force coefficient D^* (d) as functions of λ for various values of P at $A = 1$, $B = 1$, $\zeta_w^* = 1$, and $\kappa a = 1$.

of the cavity λ $(= a/b)$ are illustrated in Fig. 12. The behavior of U^* shown in Fig. 12a is more complicated than that in Fig. 9. In the former, the sign of U^* depends on the levels of P and λ. In addition, U^* may have a negative local minimum as λ varies. These can be explained by the behaviors of F_E^*, $F_{D,2}^*$, and D^* shown in Figs. 12b and 12c. As seen, $F_E^* < 0$, $F_{D,2}^* > 0$, and $D^* > 0$; if λ is small, F_E^* and $F_{D,2}^*$ dominate, and if λ is large, D^* dominates. Here, $|F_E^*|$ increases with increasing λ and/or increasing P. This is because in these cases the compression of the electric field between the particle and the cavity leads to an increase in the charge den-

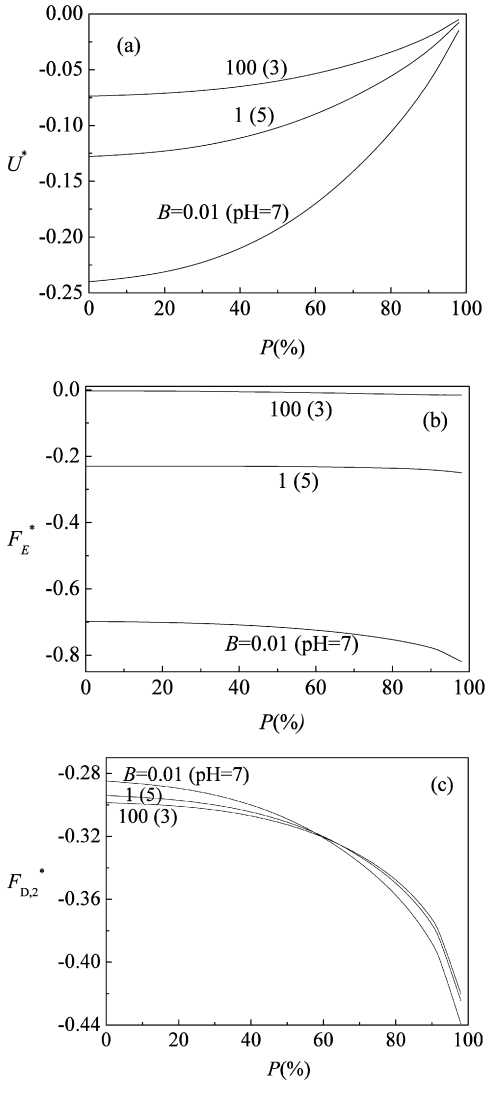

Fig. 13. Variation of the scaled mobility U^* (a), the scaled electric force F_E^* (b), and the scaled excess hydrodynamic force $F_{D,2}^*$ (c) as functions of P for various values of B (or pH) at $A = 1$, $\zeta_w^* = -1$, $\kappa a = 1$, and $\lambda = 0.4$.

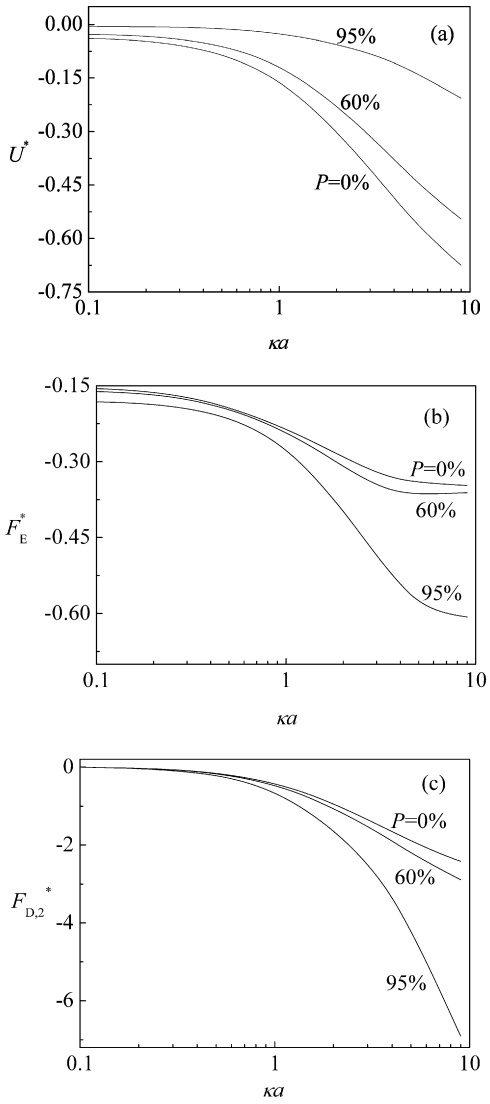

Fig. 14. Variation of the scaled mobility U^* (a), the scaled electric force F_E^* (b), and the scaled excess hydrodynamic force (c) as functions of κa for various values of P at $A = 1$, $B = 1$, $\zeta_w^* = -1$, and $\lambda = 0.4$.

sity on the particle surface, and therefore an increase in $|F_E^*|$ [5,15]. As seen in Fig. 12c, the qualitative behavior of $F_{D,2}^*$ at $P = 0\%$ and 60% is dissimilar to that at $P = 95\%$. This arises from the competition between $F_{D,2(v)}^*$ and $F_{D,2(P)}^*$ [5,15,16]. If the boundary effect is important (λ and/or P are large), $F_{D,2}^*$ is dominated by $F_{D,2(P)}^*$; on the other hand, if it is unimportant, $F_{D,2}^*$ is dominated by $F_{D,2(v)}^*$ [5,15,16]. As mentioned previously, the rapid increase in D^* at large λ and P seen in Fig. 12d arises from the nonslip condition on the cavity surface.

3.3. Charge-regulated sphere in a negatively charged cavity

Let us consider next the case where a charge-regulated sphere is in a negatively charged cavity. Fig. 13a indicates that the qualitative behavior U^* as P and B vary is similar to that observed in Fig. 4a, and can be explained by the same reasoning. Note that the variation of D^* as P and B vary is the same as that shown in Fig. 4d. In the present case, because the negatively charged cavity yields a counterclockwise (clockwise) electroosmotic flow on the right- (left-)hand side of the particle, the velocity of the particle is raised. A comparison between Figs. 4c and 13c indicates that $|F_{D,2}^*|$ for the present case is greater than for the case where the cavity is uncharged; that is, the hydrodynamic force experienced by the particle is greater than that for the case where the cavity in uncharged. As seen in Figs. 13b and 13c, although the magnitudes of $F_{D,2}^*$ and F_E^* are comparable, they have the same sign, and therefore, the behavior of U^* is not as complicated as that in the case where the cavity is positively charged.

The general behavior of U^* as A and/or P varies is the same as that observed in Fig. 5. For the present case, although the positive charge is induced on the particle surface as it approaches the negatively charged cavity surface, thereby reducing the net surface charge density and the electrical driving force, the electroosmotic flow arising from the presence of the charged cavity has the effect of raising the mobility of the particle. Therefore, the behavior of A is roughly the same as that shown in Fig. 5.

The variations of the scaled mobility, U^*, and the corresponding scaled forces, F_E^* and $F_{D,2}^*$, as functions of κa are illustrated in Fig. 14. Because the positive charge is induced on the particle surface as it approaches the negatively charged cavity, and the smaller the κa the more the amount of induced charge, $|F_E^*|$, and therefore U^*, declines accordingly. As expected, the larger the P the more significant that effect is. Note that the general trend of U^* illustrated in Fig. 14a is different from that of U^* observed in Figs. 6a and 12a. This is because the order of magnitude of $F_{D,2}^*$

(positive) in Fig. 6a is roughly the same as that of F_E^* (negative), in Fig. 12a $F_{D,2}^*$ dominates (except for small κa), and both $F_{D,2}^*$ and F_E^* are negative in Fig. 12a. The trend of $F_{D,2}^*$ seen in Fig. 14c can be explained by the result of the competition between $F_{D,2(P)}^*$ and $F_{D,2(v)}^*$. As mentioned previously, if the boundary effect is significant (small κa and/or large P), $F_{D,2}^*$ is dominated by $F_{D,2(P)}^*$. On the other hand, if the boundary effect is insignificant, $F_{D,2}^*$ is dominated by $F_{D,2(v)}^*$. The dependence of U^* on P and λ is the same as that shown in Fig. 9.

4. Summary

In summary, the influence of a charged boundary on the electrophoretic behavior of a charge-regulated particle is modeled by considering the electrophoresis of a spherical particle, the surface of which contains dissociable functional groups, in a spherical cavity. We show that, due to the presence of an electroosmotic flow, the charged boundary can influence the mobility of the particle significantly, both qualitatively and quantitatively. For the case where the cavity is uncharged we conclude the following: (a) The absolute value of the mobility of the particle increases with increasing pH and with the density of the acidic functional groups on the particle surface. (b) If the particle is not too close to the cavity, the absolute value of the mobility decreases with decreasing thickness of a double layer, that is different from the corresponding behavior of a rigid particle. (c) If the particle is sufficiently close to the cavity, the mobility has a negative local minimum as the thickness of a double layer varies. If the cavity is positively charged, then the following conclusions can be drawn: (a) If pH is sufficiently high, the mobility is negative and the closer the particle to the cavity the smaller its absolute value. On the other hand, if the pH is sufficiently low, the mobility is positive, and the closer the particle is to the cavity the smaller the mobility. (b) If a double layer is thick, the mobility is negative, and its absolute value declines with decreasing double layer thickness. On the other hand, if the double layer is sufficiently thin, the mobility is positive and it increases with decreasing double layer thickness. (c) The sign of the mobility depends on the relative position in the cavity and its relative size with respect to that of the cavity. In addition, the mobility may have a negative local minimum as its relative size varies. If the cavity is negatively charged, then (a) The qualitative behavior of the mobility as its relative position in the cavity and pH vary is similar to that in the case where the cavity is uncharged. (b) The thicker a double layer the smaller the absolute value of the mobility. (c) The general trend of the mobility as the thickness of a double layer varies is different from that for the case where the cavity is uncharged or positively charged.

Acknowledgment

This work was supported by the National Science Council of the Republic of China.

References

[1] J. Ennis, J.L. Anderson, J. Colloid Interface Sci. 185 (1997) 497.
[2] A.A. Shugai, S.L. Carnie, J. Colloid Interface Sci. 213 (1999) 298.
[3] J.P. Hsu, M.H. Ku, C.C. Kuo, Langmuir 21 (2005) 7588.
[4] A.L. Zydney, J. Colloid Interface Sci. 169 (1995) 476.
[5] J.P. Hsu, L.H. Yeh, Z.S. Chen, J. Colloid Interface Sci. 310 (2007) 281.
[6] H.Y. Yu, S.H. Hung, J.P. Hsu, Colloid Polym. Sci. 283 (2004) 10.
[7] C.P. Tung, E. Lee, J.P. Hsu, J. Colloid Interface Sci. 260 (2003) 118.
[8] E. Lee, J.W. Chu, J.P. Hsu, J. Colloid Interface Sci. 205 (1998) 65.
[9] J.P. Hsu, S.H. Hung, C.Y. Kao, Langmuir 18 (2002) 8897.
[10] S.H. Lou, E. Lee, J.P. Hsu, J. Colloid Interface Sci. 285 (2005) 865.
[11] J.P. Hsu, L.H. Yeh, M.H. Ku, J. Colloid Interface Sci. 305 (2007) 324.
[12] J.P. Hsu, L.H. Yeh, J. Chin. Inst. Chem. Eng. 37 (2006) 601.
[13] R.B. Bird, R.C. Armstrong, O. Hassager, Dynamics of Polymer Liquids, vol. 1, Wiley, New York, 1987.
[14] G. Backstrom, Fluid Dynamics by Finite Element Analysis, Studentlitteratur, Lund, Sweden, 1999.
[15] J.P. Hsu, M.H. Ku, C.Y. Kao, J. Colloid Interface Sci. 276 (2004) 248.
[16] J.P. Hsu, M.H. Ku, J. Colloid Interface Sci. 283 (2005) 592.
[17] J.P. Hsu, C.Y. Kao, J. Phys. Chem. B 106 (2002) 10605.
[18] R.W. O'Brien, L.R. White, J. Chem. Soc. Faraday Trans. 2 74 (1978) 1607.
[19] FlexPDE Version 2.22, PDE Solutions Inc, USA, 2000.
[20] Y.P. Tang, M.H. Chih, E. Lee, J.P. Hsu, J. Colloid Interface Sci. 242 (2001) 121.